Physics of Fluids

RESEARCH ARTICLE | JANUARY 07 2025

Alginate biopolymer viscoelasticity from sol to gel: Linear and nonlinear rheology, and Brownian motion of tracer particles embedded in the polymer network

Special Collection: Kitchen Flows 2024

Ricky F. López-Santiago ; Rolando Castillo

Physics of Fluids 37, 013110 (2025)
https://doi.org/10.1063/5.0245878

Physics of Fluids ARTICLE pubs.aip.org/aip/pof

Alginate biopolymer viscoelasticity from sol to gel: Linear and nonlinear rheology, and Brownian motion of tracer particles embedded in the polymer network

Cite as: Phys. Fluids **37**, 013110 (2025); doi: 10.1063/5.0245878
Submitted: 29 October 2024 · Accepted: 9 December 2024 ·
Published Online: 7 January 2025

Ricky F. López-Santiago and Rolando Castillo[a)]

AFFILIATIONS

Instituto de Física, Universidad Nacional Autónoma de México, P.O. Box 20-364, 01000 Mexico City, México

Note: This paper is part of the Special Topic: Kitchen Flows 2024.
[a)]**Author to whom correspondence should be addressed:** rolandoc@fisica.unam.mx

ABSTRACT

The linear and nonlinear rheological behavior of alginate/Ca^{2+} gels made through slow solubilization of $CaCO_3$ using gluconic acid-δ-lactone was studied. Rheological modulus follows a power law at the critical point; exponents ($n = 0.60$–0.65) decrease slightly, increasing Ca^{2+} ions. These values agree with those reported in the literature with similar mannuronic/guluronic residue ratios and total polymer concentration. The strain-hardening behavior of matured gels was investigated using large amplitude oscillatory shear. The Blatz–Sharda–Tschoegl scaling model was used to estimate their fractal dimension, whose values were 1.23–1.31; the fractal dimension is not sensible to Ca^{2+} concentration. The Lissajous–Bowditch curves show a higher nonlinearity and constitute a rheological fingerprint of these gels. The geometrical decomposition of intracycle strain in terms of strain thickening and stiffening ratios shows a weak formation of temporary network junctions during the breaking process due to the convexity of their curves. Diffusion wave spectroscopy was used to determine the mean square displacement of microspheres embedded in polymer solution exhibiting a subdiffusive process, with two slopes: $m \sim 0.3$ at short times and $m \sim 1$ at long times. The diffusive region section decreases as the gelation progresses due to Ca^{2+} and disappears when gels are formed. Gelation time was estimated to identify a terminal relaxation time, whose evolution follows almost the same exponential curve for gels with high Ca^{2+} concentration due to the formation of many multiple egg-box structures. After 24 h of gelation, mean square displacement curves show an apparent plateau, indicating important particle confinement.

I. INTRODUCTION

Alginates are polysaccharide biomolecules extracted from brown seaweed and some bacteria.[1–3] Alginates are notable for their biocompatibility, non-toxicity, and biodegradability, making them suitable for pharmaceuticals, bioengineering, and the food industry.[3–8] In the food industry, alginate applications are based on three main properties: (1) thickening, (2) gelling in the presence of calcium salt, and (3) film-forming properties.[4,8] As a functional food ingredient, alginate is a food additive that enhances food preservation and improves flavor, taste, and appearance. Thickening is helpful for sauces, sirups, and cream toppings and also is useful for stabilizing water-in-oil emulsions like mayonnaise and dressings. Gelling is useful for different food products such as milk desserts, jellies, bakery filling creams, animal foods, and reformed fruit.[4,8]. It forms heat-stable gels at low temperatures, which is beneficial for restructuring food items sensitive to high temperatures, such as fish, fruits, and vegetables [4,9]. Additionally, alginate can enhance the visual appeal of foods and enable the creation of innovative products in various shapes and sizes.

Alginate is an anionic linear copolymer of (1→4)-linked β-L-mannuronic (M) and α-L-guluronic (G) residues.[3,7] The residues are arranged randomly with GG, MM, and GM-dimer blocks spread along the polymer chain, as shown in Fig. S1(a) in the supplementary material. The MM block forms a β-1,4-glycosidic bond, forming a linear flexible local structure, while the GG block forms an α-1,4-glycosidic bond, introducing steric hindrance space around the carboxyl groups. So, the GG block provides a folded and rigid structural conformation responsible for the alginate chain's significant stiffening. The stereochemistry of the GG block enables alginate chains to create a gel

when exposed to divalent cations, such as Ca^{2+}. This occurs by forming a highly stable crosslinked structure called the "egg box."[10–13] In this simple egg-box structure, two GG blocks from two alginate chains are linked by a divalent ion by coordinating carboxylic groups [see Fig. S1(b) in the supplementary material]. GG blocks may favor the egg-box structure, which is also called rod-like links.[11,12] The mechanical properties of alginate gels are determined by various physiochemical parameters, such as the M/G ratio, molecular weight, and concentrations of polymer and Ca^{2+} ions.

The Ca-alginate gelling process methods include external or internal gelation, with the main difference being the method for introducing Ca^{2+}.[10,13,14] In the internal gelation, alginate exposure to Ca^{2+} is controlled to achieve a uniform distribution; first, an insoluble calcium salt, such as $CaCO_3$ or $CaSO_4$, is added to a solution of sodium alginate, and then, an acidifier is added to the mixture, releasing Ca^{2+}, usually is used glucono-δ-lactone.[15–17] In the external gelation method, Ca^{2+} is diffused from a higher concentration region into the alginate interior, allowing for the rapid formation of gel.[10,17] These gelation methods allow the encapsulation of reactive or volatile molecules, e.g., acidulants, fats, and flavors, and live probiotic cells for food and drug delivery to the large human bowel.[9,18–20]

The linear viscoelastic behavior of solutions and gels made of alginate and its dependence on physicochemical parameters have been extensively studied, as well as the transition from sol to gel state, where the transition point is called the gel point,[21,22] or the critical gel.[23] Several studies of physical and chemical gels using SAOS (small amplitude oscillatory shear) indicate that the elasticity modulus, $G'(\omega)$, and viscous modulus, $G''(\omega)$, follow a power law in the critical point with the angular frequency ω,

$$G'(\omega) \sim G''(\omega) \sim \omega^n, \text{ and } \delta = \tan^{-1}(n\pi/2). \tag{1}$$

Here, n is a critical exponent similar to those in critical phenomena,[21,22,24,25] and δ is the loss angle, $\tan\delta = G''(\omega)/G'(\omega)$. The relaxation modulus, $G(t)$, is related to the complex modulus, $G^* = G'(\omega) + iG''(\omega)$; then, $G(t) = \mathfrak{F}^{-1}\{G^*(\omega)/i\omega\} = S_n t^{-n}$. S_n, the gel strength, and n are obtained by experimental fitting. At the gel point, the diverse rheological material properties reach a universal dynamic state of less complexity. The critical exponent can be determined theoretically using the percolation theory.[24,25] The reported critical exponents for most physical gelations are not universal; they vary from 0.11 to 0.8,[21] depending on the stoichiometry, molecular weight, and bonding mechanism. For alginate gels cross-linking with different divalent cations, n varies slightly around ~0.21–0.76.[26–31]

Recently, a point of interest is the nonlinear rheological characterization of gelling materials and their relationship with their structure.[32–34] Beyond the linear regimen, the viscoelasticity moduli are not independent of the applied strain, and drastic reconfiguration of mesoscopic structure occurs, contributing substantially to the mechanical response. Various mechanical processes, such as food processing, packaging, biting, swallowing, and chewing, can be understood by LAOS (large amplitude oscillatory shear) experiments where the shear amplitude is large, allowing us to explore a wide range of timescales and deformation strengths. LAOS has been used for nonlinear viscoelasticity characterization of food, e.g., cheeses,[35] yogurts,[36] cool whips,[37] chocolates,[38] and blenders of polysaccharides and proteins.[39–41] Recently, Goudoulas *et al.*[42] reported that a nonlinear rheological response of a layer of alginate/Ca^{2+} gels shows an overshoot in the viscous modulus, similar to gelatin-alginate layer gels.[43] Several studies have described the nonlinear rheological behavior of gels made with polysaccharides and proteins;[42–45] however, the measurements usually involve gels fabricated *ex situ*. Concerning the analysis of LAOS measurements, the most common practice is to extend the liner regimen Fourier analysis to higher harmonics.[34,46,47] When the applied shear strain is sinusoidal, expressed as $\gamma = \gamma_0 \sin \omega t$, where γ_0 represents now a large strain amplitude and ω is the frequency, the shear stress is an odd function of the shear direction, i.e., $\sigma[-\gamma(t), -\dot{\gamma}(t)] = -\sigma[\gamma(t), \dot{\gamma}(t)]$, where $\dot{\gamma}(t)$ is the shear rate of strain $[\dot{\gamma}(t) = \gamma_0\omega\cos(\omega t)]$. Then, the nonlinear stress can be represented entirely by only odd harmonics with odd symmetry due to the directionality of shear strain or shear rate just mentioned,

$$\sigma(t;\omega,\gamma_0) = \gamma_0 \sum_{n\,odd} \left\{ G'_n(\omega,\gamma_0)\sin(n\omega t) + G''_n(\omega,\gamma_0)\cos(n\omega t) \right\}, \tag{2}$$

where G'_n and G''_n are the nonlinear elastic and viscous moduli, respectively.[34,48] Graphically, changes in shear stress due to the higher harmonics contribution can be visually observed through the Lissajous–Bowditch (LB) curves,[34] which are 3D curves $[\sigma/\sigma_o$ vs γ/γ_o and $\dot{\gamma}/(\gamma_o\omega)]$ and by their projections [elastic representation: σ/σ_o vs γ/γ_o or viscous representation: σ/σ_o vs $\dot{\gamma}/(\gamma_o\omega)$]. Also, the strain-hardening behavior in the nonlinear viscoelasticity region can provide relevant information about the fractal dimension of the network by fitting the experimental data to the BST (Blatz, Sharda, and Tschoegl) – scaling model.[49,50]

In addition to rheometry, microrheology has been used to measure the viscoelasticity properties in polymer solutions, critical gels, and aging gels of different biopolymers gels.[51–59] The general principle behind microrheology is to minimize the mechanical probe that deforms the medium. This probe could be a colloidal microsphere. The material's properties can be determined by tracking the motion of the thermally fluctuating probes, which is affected by the viscoelasticity of the medium. Diffusing wave spectroscopy (DWS) allows the measurement of the mean square displacement (MSD) of the colloidal probe, and the viscoelasticity materials' properties at high frequencies can be obtained from it, spanning micrometer and sub-micrometer scales through DWS-microrheology equations.[60,61] Unlike rheometry, the material's strain might be almost non-existent during measurements because of the small size of the probes. This is useful when studying the gelling process since even minor applied strains can cause structural reorganization and alter the viscoelastic properties of the material. DWS-microrheology has been used to analyze the kinetic gelation of physical, chemical, and hybrid gels in gelatin solutions.[55] By analyzing the high-frequency viscoelasticity spectra, changes in the network's mesh size and the persistence length of the unbonded flexible polymer section can be followed during gelation.

In this work, we offer a systematic study of the gelation process of alginate. We establish correlations between rheological properties and mesoscopic parameters at different stages, from polymer solution to mature gel. We want to answer some questions: Does the critical exponent for critical gels change by varying the Ca^{2+} concentration? How is the fractal dimension in mature gels modified with the Ca^{2+} concentration? Does the Ca^{2+} concentration modify the mechanical nonlinear viscoelastic response? How do the MSDs of tracer particles change during gelation?

Chemical products used to form the alginate/Ca^{2+} gels are categorized by the U.S. Food & Drug Administration (FDA) as generally

recognized as safe (GRAS) products, and their concentrations are far from the median lethal dose; the gels studied in this work are safe for human consumption. In general, the applications of gels in the food industry need extensive comprehension of formation mechanisms to enable a deeper understanding and accurate prediction of the gelation progress, particularly because they present an intricate interplay of structure, dynamics, and rheological properties. This complexity makes it exciting to predict their response to shear stress. Therefore, real-time recording of gelation kinetics, such as those provided by microrheology, can produce valuable insights into the cross-linking reactions of alginate gels during gelation. Oscillatory time sweeps can be used to study the temporal evolution of the mechanical properties of gels undergoing time-dependent structural rearrangements, particularly when different classes of gels are prepared with nearly identical linear rheology but significantly different yield transitions and nonlinear properties at post-yielding. With the advancement of living standards, demands for nutritious, safe, reliable, and functionally diverse foods have increased. As a result, gels exhibiting unique advantages for food applications will be of great significance. We expect that the nonlinear viscoelastic response and its link to the microstructure discussed here could help understand food processing issues.

II. EXPERIMENTAL SECTION

A. Materials

Sodium alginate from brown algae [Mol. Wt. 324 138 Da, mannuronic residue to the guluronic residue (M/G) ≈ 1.56, Sigma-Aldrich USA], calcium carbonate ($CaCO_3$, purity > 99.0%, Sigma-Aldrich USA), and D-(+)-gluconic acid δ-lactone (GDL, purity > 99.0%, Sigma-Aldrich USA) were used. Solutions were prepared with ultrapure de-ionized water (NaNoPure, USA), and the chemical products were used as received. The molecular weight of alginate was determined using the Mark–Houwink–Sakurada (MHS) equation.[62] The moisture of alginate is 10.44%.

B. Gel preparation

Alginate was dissolved in ultrapure de-ionized water under magnetic stirring at ∼30 °C overnight. Then, $CaCO_3$ was dispersed in the alginate solution under vigorous vortex stirring for ∼1 min, and subsequently, GDL was added to the mixture under vortex stirring to promote the gelation mechanism. The alginate concentration was fixed ($C_{alginate} = 1.8\%$), and the quantity of $CaCO_3$ and GDL was varied ([$CaCO_3$] = 0.3, 0.4, and 0.7 mM, and $C_{GDL} = 6$–18 mg/mL). GDL is a slowing-down acidification substance promoting the solubilization of $CaCO_3$. The solubility equilibrium of $CaCO_3$ is given by $CaCO_{3(s)} \leftrightarrows Ca^{2+} + CO_3^{-2}$ (solubility constant of $K_s = 10^{-6.05}$);[63] due to the release of H^+ groups from GDL, carbonic acid (H_2CO_3) is produced ($H_2CO_3 \leftrightarrows 2H^+ + CO_3^{-2}$), and the solubilization of $CaCO_3$ takes place. In this way, it is possible to obtain a slow Ca^{2+} source for studying the gel formation from sol to gel through different stages; in contrast to alginate gels formed with $CaCl_2$, where using $CaCl_2$, the gelation is too fast due to the instantaneous solubilization of Ca^{2+}.[10,17,26]

C. Rheological measurements

SAOS and LAOS protocol measurements were performed with an MCR-702 Twin Drive rheometer (Anton Paar, Austria) using a cone-plate geometry (2° cone angle, Diam. = 40 mm) with temperature control (±0.1 °C). A solvent trap was used to avoid water evaporation.

1. Estimation to reach the gel-point time and viscoelastic spectra at the gel point

An estimation of the gelation time is given by the time needed to reach the gel point, i.e., the elapsed time to reach $G'(t) \sim G''(t)$ along an isothermal time sweep experiment with a constant frequency ($\omega = 0.5$ rad s^{-1}) and a constant strain ($\gamma = 0.8\%$), i.e., in the linear viscoelasticity region (LVR). The viscoelastic spectra are determined after starting the gelation process. The viscoelastic spectra are measured for a wide range of frequencies, $\omega = 0.2$–350 rad s^{-1} at fixed strain ($\gamma = 0.8\%$). All measurements are made at 25 °C and performed at least twice.

2. Linear and nonlinear viscoelastic response of mature gels

The nonlinear viscoelastic response is obtained on matured gels after 5–6 h of starting the gelation process. It is considered a matured gel when the viscoelastic moduli do not change with time for at least 30 min in an isothermal time sweep experiment ($\omega = 0.5$ rad s^{-1} and $\gamma = 0.8\%$ are fixed). Frequency sweep measurements are carried out in the range of $\omega = 0.1$–100 rad s^{-1} in the LVR ($\gamma = 0.8\%$). Afterward, strain-sweep measurements are developed in a wide range of strains for LAOS measurements, $\gamma_0 = 0.1\%$–5000% ($\omega = 1$ rad s^{-1}). Lissajous–Bowditch curves are obtained for one imposed intracycle shear strain. All measurements are made at 25 °C and performed at least twice.

D. Diffusive wave spectroscopy (DWS) and microrheology

The mean square displacement (MSD, $\langle \Delta r^2(t) \rangle$) of microspheres embedded in alginate solutions is measured using the DWS technique. The connection between MSDs and complex modulus is given by a generalized Stokes–Einstein (GSE) relationship, $\tilde{G}(s) = k_B T / \pi a s \Delta \tilde{r}^2(s)$,[60,61] where $\tilde{X}(s)$ denotes the Laplace transform in s-space of $X(r)$, k_B is Boltzmann's constant, T is the absolute temperature, and a is the radius of microspheres. A recent review describes our homemade DWS setup in detail.[60] Polystyrene (PS) microspheres (dia. 784 nm, vol. fraction ∼0.025; Bangs Labs, USA) were added to the alginate/$CaCO_3$ solutions and mixed under vigorous vortex stirring. Subsequently, a fresh aliquot of GDL was added, mixed, and placed in a rectangular optical glass cuvette (∼2 mm optical-path length, Sterna Cell, Inc.) at 25 °C. The gelation process of alginate starts when GDL is added to the alginate/$CaCO_3$/PS microspheres solution and mixed; this time corresponds to the starting point of the gelation process for measuring the MSDs. The elapsed time since the GDL addition will be referred to as t_q. The MSDs of probe microspheres are determined by collecting their scattered light from a speckle over 180–300 s, and the intensity auto-correlation function is evaluated; scattered light collected for 180 s is enough to consider local thermodynamic equilibrium with good statistics. After gelation starts, measurements are taken along ∼8 h for different t_q. From the MSD, the viscoelastic spectra can be evaluated up to high frequencies ($\omega \approx 10^2$–10^6 rad s^{-1}), as shown for living polymers[64–67] and gels.[55,68] The experimental MSD curves for the sol state are fitted using a power law with two terms ($\langle \Delta r^2(t) \rangle = A_1 \cdot t^{\alpha_1} + A_2 \cdot t^{\alpha_2}$, where A_1, A_2, α_1, and α_2 are fitting constants).

III. RESULTS AND DISCUSSION

A. Linear viscoelasticity spectra around sol-gel transition

The GDL concentration was chosen in such a way that the gelation process was slow enough to allow time to make accurate measurements using mechanical rheology close to the gel point. Gelation time was estimated as described in Sec. II C 1. The results are shown in SM2a, where the gelation time can be identified by the intersection of $G'(t, \omega_0)$ and $G''(t, \omega_0)$ with $\omega_0 = 0.5$ rad s^{-1}. Gelation times for GDL concentrations of 6, 12, and 18 mg/mL, with fixed $[CaCO_3] = 3$ mM, were found to be ∼143, ∼59, and ∼41 min, respectively. Therefore, a GDL concentration of 6 mg/mL was chosen to study critical gels. In the studied gels, Ca^{2+} concentration was varied, i.e., $[CaCO_3] = 3$, 5, and 7 mM. Figure 1 shows the viscoelastic moduli close to the gel point; we use various vertical scales (y-axes) in different colors to accommodate all measurements in a single figure. The time delay before the current start of the viscoelastic spectra measurements ($G'(\omega)$, and $G''(\omega)$ vs ω) close to the gel point was estimated with isothermal time sweep experiments [see Fig. S2(b) in the supplementary material]. According to Chambon and Winter criteria,[22,23] the critical points $G'(\omega)$ and $G''(\omega)$ are parallel along more than three orders of magnitude in frequency, i.e., $G'(\omega)$ and $G''(\omega) \sim \omega^n$ with $n = 0.60$–0.65, whereas as $[Ca^{2+}]$ increases, the critical exponent decreases slightly. Liu *et al.*[28] showed the same dependence between n and $[Ca^{2+}]$. They associated this behavior with a corresponding increase in the junction density as $[Ca^{2+}]$ increases, leading to a slight reduction of n. This behavior is similar to the case of chemical gels, where an increase in cross-linking leads to a decrease in n.[28]

The rheological properties are intimately related to the network's structure close to the gel point. According to the percolation theory, the divergence of the shear zero viscosity and elastic modulus close to the gel point can be expressed as power law behavior,

$$\eta_0 \sim \left(\frac{|p - p_c|}{p_c}\right)^{-k} \text{with } p < p_c, \tag{3}$$

$$G_0 \sim \left(\frac{|p - p_c|}{p_c}\right)^{z} \text{with } p > p_c, \tag{4}$$

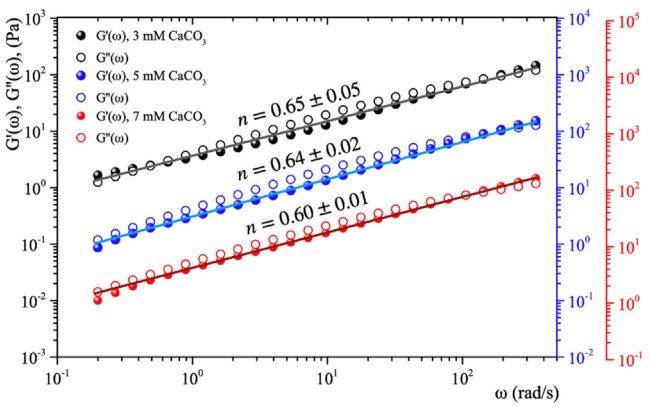

FIG. 1. Linear viscoelastic spectra [$G'(\omega)$, $G'(\omega)$ vs ω] close to gel point for alginate critical gels ($C_{alginate} = 1.8$ w/v % and $C_{GDL} = 6$ mg/mL) varying the $[CaCO_3] = 3$, 5, and 7 mM at 25 °C. Experiments performed at $\gamma_0 = 0.8\%$.

where k and z are critical exponents, where the critical exponents are related to $n = z/(k + z)$. Martin *et al.*[69] described the sol-gel transition phenomena by distributing relaxation times for branched polymers in a dilute concentration regimen. They found $k = 1.33$ and $z = 2.67$, so $n = 0.667$, which is close to our n values. This result suggests that the percolation network of the gel under study here is similar to that of branched polymers.[69] Experimentally, for alginate critical gels, different values of n are reported by several authors, as shown in Table I. Our results agree with the n values reported for similar M/G ratios and $C_{alginate}$. It is important to note that the dispersion of n shows a strong dependence on the nature of the alginate chain, e.g., M/G ratio, polymer concentration ($C_{Alginate}$), and molecular weight (M_W), as well as the nature of divalent ions and the network's structure around the gel point.

B. Strain hardening of matured gels and fractal dimension

As mentioned in Sec. II C 2, rheological measurements of matured states correspond to those where the viscoelastic moduli do not change over time for at least 30 min in isothermal time sweep experiments (see Fig. S3 in the supplementary material); on average, the rheological measures started ∼5–6 h after starting the gelation process. For all matured gels, the linear viscoelasticity spectra show a solid-like behavior [$G'(\omega) > G''(\omega)$] in a wide range of frequency, $\omega = 0.1$–100 rad s^{-1} (see Fig. S4 in the supplementary material). Figure 2 shows the $G'(\gamma_o)$ and $G''(\gamma_o)$ vs γ_o for different matured gels in a wide range of strain, 0.1%–5000%, for a fixed frequency ($\omega = 1$ rad s^{-1}). Here, $G'(\gamma_o)$ and $G''(\gamma_o)$ exhibit a similar trend, which could be

TABLE I. Critical exponents for alginate critical gels made with different alginates crosslinked with several ions.

Gel system	$M_w \times 10^4$ (Da)	M/G	$C_{Alginate}$ (Wt %)	n	Ref.
Alginate/Ca^{2+}	32	1.56	∼1.8	0.60–0.65	Our results
Alginate/Ca^{2+}	62	0.6	2–6	0.72–0.68	26
	330	0.91	2	0.72	
			3	0.50	
			4–6	0.37	
Alginate/Ca^{2+}	41	0.6	3	0.689	27
	122	1.85		0.620	
	323	1.85		0.580	
	349	0.91		0.562	
Alginate/Ca^{2+}	10–15	1.67–2	2	0.756	28
			3	0.728	
			4	0.694	
			5	0.666	
Alginate/Cu^{2+}	21	1	1	0.678	29
Alginate/Cu^{2+}	62	0.6	1	0.6	30
	122	1.85		0.65	
	323	1.85		0.66	
	330	0.91		0.5	
Alginate/Fe^{2+}	10–20	···	1	0.21	31

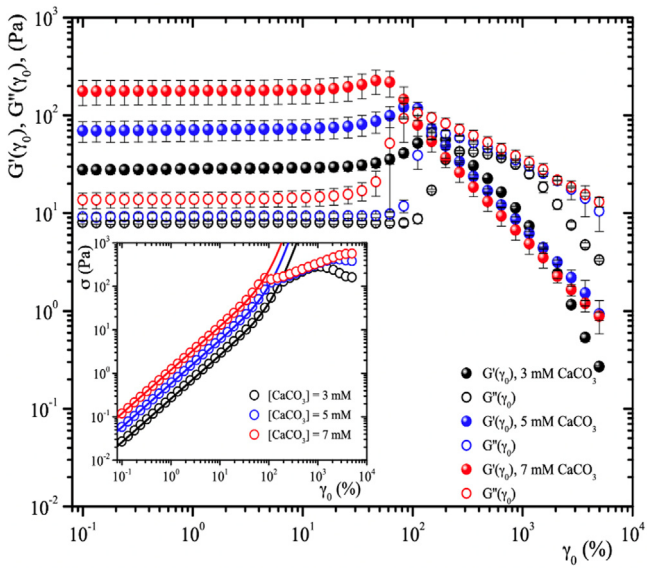

FIG. 2. $G'(\gamma_o)$ and $G''(\gamma_o)$ vs γ_o for alginate matured gels ($C_{alginate} = 1.8$ w/v % and $C_{GDL} = 6$ mg/mL) varying the $[CaCO_3] = 3$, 5, and 7 mM at 25 °C. Inset: σ vs γ_o, and the fittings to the BST model (continuous line, $R^2 > 0.99$ for all cases). Experiments performed at $\omega = 1$ rad s^{-1}.

described with three regions as in the case of gelatin matured gels.[55] In the linear viscoelastic region, $G'(\gamma_o)$ and $G''(\gamma_o)$ are constant with $G'(\gamma_o) > G''(\gamma_o)$. In a second region, $G'(\gamma_o)$ and $G''(\gamma_o)$ increase with a positive curvature strain. A sudden overshoot produces a third region where $G'(\gamma_o)$ and $G''(\gamma_o)$ decrease as the strain increases until reaching a crossing point $G'(\gamma_o) \sim G''(\gamma_o)$, suggesting a network failure point where it starts to break. As γ_o increases, $G''(\gamma_o) > G'(\gamma_o)$, which is related to the flow of a broken gel, as will be discussed below. The overshoot can be easily seen in the σ vs γ_0 curves in the inset of Fig. 2.

We used the BST-scaling model to determine the fractal dimension to fit the nonlinear viscoelastic data to obtain information about the gel network's microstructure. BST proposed a model involving a non-Hookean relation between deformation energy and deformation.[49] For an applied shear stress, the relationship to the shear stress is

$$\sigma = \frac{2G_0}{n_{BST}} \frac{\lambda^{n_{BST}} - \lambda^{-n_{BST}}}{\lambda - \lambda^{-1}}, \tag{5}$$

where $\lambda = 1/2\,\gamma_o + \left(1 + 1/4\,\gamma_o{}^2\right)^{1/2}$ (or $\gamma_o = \lambda - \lambda^{-1}$), G_0 is the elasticity modulus ($G_0 = \lim_{\gamma_o \to 0} G'(\gamma_o)$), and n_{BST} is a nonlinear fitting exponent. Interestingly, for $n_{BST} = 2$, the last equation reduces to the ideal rubber elasticity case: $\sigma = G\gamma_o$. A molecular interpretation of n_{BST} was developed by Groot *et al.*[50] using scaling arguments. The fractal dimension of the network, d_f, of the network could be related to the BST model as

$$n_{BST} \approx \frac{d_f}{d_f - 1}. \tag{6}$$

The fittings of σ vs γ_o curves correspond to the continuous lines in the insets of Fig. 2 ($R^2 > 0.99$ for all cases; R is the regression coefficient). Table II presents all parameters for the BST scaling model and strain breaking.

For alginate-matured gels, G_0 increases as the concentration of Ca^{2+} increases. With $[Ca^{2+}] = 3$ mM, the elastic modulus is ~ 27 Pa; this modulus increases almost by one order of magnitude for $[Ca^{2+}] = 7$ mM, suggesting that as the amount of calcium increases, the density of cross-linking points also increases, which agrees with the results of the last section (Sec. III A). On the contrary, γ_{break} decreases as the concentration of $[Ca^{2+}]$ increases. The network formed with $[Ca^{2+}] = 7$ mM requires a lower strain to be broken than the gel structure formed with 3 mM of $[Ca^{2+}]$ as if it were more brittle as $[Ca^{2+}]$ increases. The physical mechanism to break the alginate gels seems to involve an unzip mechanism of two alginate chains.[12,13,42] Larobina *et al.*[12] reported that alginate gels present multi egg-box structures by slowly hydrolyzing $CaCO_3$, using GDL, resulting in rod-like junctions and bundles of several chains. Therefore, as Ca^{2+} increases, there are more multi egg-box structures, explaining the relationship between γ_{break} and calcium. However, the alginate-matured gel fractal dimension is not sensible to the $[Ca^{2+}]$ concentration. Our results for d_f agree well with those reported by Posbeyikian *et al.*[70] for alginate beads. Using SAXS experiments, they reported a fractal dimension of 1.25 for alginate beads formed in a calcium solution of $[CaCl_2] = 100$ mM. The relationship between the d_f and $[Ca^{2+}]$ concentration indicates that the self-similarity of the mature network essentially does not change with the amount of added $[Ca^{2+}]$; on amplification, statistically, we must observe the same surrounding structure.

C. Lissajous–Bowditch curves and nonlinear decomposition

1. Alginate solution

Figure 3 shows the nonlinear response of $G'(\gamma_o)$ and $G''(\gamma_o)$ vs γ_o for alginate solution in a wide strain range (0.1%–5000%) for a fixed ω (=1 rad s^{-1}). These spectra show two regions: In the first one, $G'(\gamma_o)$ and $G''(\gamma_o)$ are constant with $G''(\gamma_o) > G'(\gamma_o)$ when $\gamma_o \lesssim 46\%$, and in the second region, $G'(\gamma_o)$ and $G''(\gamma_o)$ decrease with a negative curvature as strain increases. Here, alginate solutions exhibit shear thinning, apparently due to chain alignment along the flow direction.[34] Previous reports found that as the shear rate increases ($\dot{\gamma}_0 = \gamma_0\omega$; $\dot{\gamma}_0$ is the maximum shear rate for an intracycle shear strain), the flow alignment

TABLE II. Parameters associated with BST scaling model and γ_{break} for alginate matured gels.

	G_0 (Pa)	n_{BST}	d_f	γ_{break} (%)
$[CaCO_3] = 3$ mM	27.07 ± 2.46	4.25 ± 0.002	1.31 ± 0.001	149 ± 0.0
$[CaCO_3] = 5$ mM	69.88 ± 16.66	4.97 ± 0.48	1.25 ± 0.03	97.0 ± 19.8
$[CaCO_3] = 7$ mM	177.19 ± 49.98	5.46 ± 0.50	1.23 ± 0.03	63.7 ± 18.5

increases, and the shear viscosity decreases further.[71] Figure 3 inset shows $G'(\omega)$, $G''(\omega)$ vs ω ($\gamma = 0.8\%$) in the LVR, where spectra show a liquid-like behavior [$G'(\omega) < G''(\omega)$]. At low frequencies (<10 rad s^{-1}), the viscoelasticity moduli exhibit a power law behavior with ω; $G'(\omega) \sim \omega^{3/2}$, and $G''(\omega) \sim \omega$. The viscous modulus aligns well with the Rouse–Zimm polymer theory ($G''(\omega) \sim \omega$), and the elastic modulus deviates from theory ($G'(\omega) \sim \omega^2$).[24] This deviation may be attributed to the wide molecular weight distribution of the sample.[27] Measurements at $\omega < 0.1$ rad s^{-1} are unreliable since noise is relatively high.

2. Alginate solution and matured gels with different content in [Ca^{+2}]

Figure 4 shows the normalized 3D Lissajous–Bowditch curves (in red) and their projections in the elastic representation (σ/σ_0 vs γ/γ_0) in green and viscous representation (σ/σ_0 *vs.* $\dot{\gamma}/\dot{\gamma}_0$) in blue for an alginate solution and three matured gels with different content in Ca^{2+}. Here, σ_0, γ_0, and $\dot{\gamma}_0 (= \gamma_0\omega)$ are the maximum shear stress, shear strain, and shear rate in an oscillation cycle, respectively. Diagrams with a blue shadow indicate the LB curves corresponding to an imposed strain of $\gamma_0 = \gamma_{break}$, and diagrams with a green shadow correspond to LB curves for a γ_0 where $G'(\gamma)$ is approximately close to $G''(\gamma)$ (see Fig. 2). The elastic and viscous representation loci for alginate solutions in the linear viscoelastic regime are essentially a circle or a diagonal line, respectively. Outside the linear regime, the alginate solution shows no significant deformation in the LB curves. However, when γ_o is greater than 642% in the viscous representation, the diagonal lines slightly bend close to $\sigma/\sigma_0 = \pm 1$.

For matured gels, the change of the elastic curves when Ca^{2+} and γ_0 are varied is quite complex, as observed in Fig. 4. Below a $\gamma_0 \sim 14\%$, gels behave according to the linear regime (see Fig. 2). At $\gamma_0 = 14.3\%$,

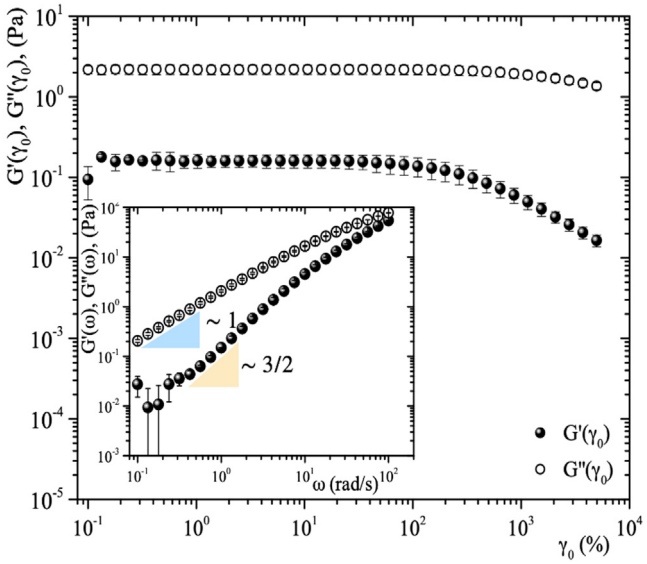

FIG. 3. $G'(\gamma_o)$ and $G''(\gamma_o)$ vs γ_o for alginate solution with $C_{alginate} = 1.8$ w/v % at 25 °C; experiments were performed at $\omega = 1$ rad s^{-1}. Inset: $G'(\omega)$, $G'(\omega)$ vs ω at fixed strain $\gamma_0 = 0.8\%$, and crosses indicate the error bar.

the LB curves are ellipses. The area of these ellipses decreases as Ca^{2+} ions increase (first row); actually, they tend to form a diagonal line, indicating that the elastic contribution in these gels increases with Ca^{2+} ions, which agrees with the increment of $G'(\gamma)$ over $G''(\gamma)$ when the Ca^{2+} concentration increases (see Fig. 2). The elastic contribution in these gels can also be observed in the circular curves presented in the viscous representation. When γ_0 is varied (vertical columns) and $<\gamma_{break}$, the loci in the viscous and elastic representations are deformed. Circles become rhomboid-like in the viscous representation, and the slim ellipses deform with a shoulder-like shape in the elastic representation. At γ_{break}, in the viscous representation, the rhomboid-like curves begin to rotate rightward. For $\gamma_{break} < \gamma_0 \lesssim \gamma_0$ (where $G'(\gamma_0) \sim G''(\gamma_0)$), the rhomboid-like curves tend toward a parallelogram-like shape, which is a characteristic of the LAOS behavior of yield stress fluids,[72] and as γ_0 increases, these shapes are entirely deformed. The loci change and widen in the elastic representation, increasing viscous dissipation.[73] Goudoulas *et al.*[42] obtained the nonlinear spectrum of alginate/Ca^{2+} gels created *ex situ* ($C_{alginate} = 2$ wt. %, $[CaCl_2] = 100$–200 mM); they show that their LB curves for alginate layers, are different from ours, indicating that the protocol used to prepare alginate gels influences the nonlinear rheological behavior. Our LB curves are similar at the higher strain ($\gamma_0 = 4980\%$, lowest row), indicating a destroyed gel network independent of Ca^{2+} concentration. The shape of these LB curves is similar to that of the alginate solution, indicating that the broken gel has nonlinear rheological properties comparable to that of the precursor solution.

A comprehensive framework is needed for quantifying, in a physically meaningful way, the nonlinear viscoelastic response of these gels that arises from the imposed deformation protocol where the strain amplitude is increased systematically. To that end, the nonlinear stress response must be decomposed into an elastic stress σ' and a viscous stress σ''. The total oscillatory stress is the sum of these two contributions that can be represented by Fourier and Chebyshev decompositions,[48]

$$\sigma' = \gamma_0 \sum_{n=odd} G'_n(\omega, \gamma_0) \sin n\omega t = \gamma_0 \sum_{n=odd} e_n(\omega, \gamma_0) T_n\left(\frac{\gamma}{\gamma_0}\right), \quad (7)$$

$$\sigma'' = \gamma_0 \sum_{n=dd} G''_n(\omega, \gamma_0) \cos n\omega t = \dot{\gamma}_0 \sum_{n=odd} v_n(\omega, \gamma_0) T_n\left(\frac{\dot{\gamma}}{\dot{\gamma}_0}\right). \quad (8)$$

Here, T_n is the nth-order Chebyshev polynomial of the first kind, and $e_n(\omega, \gamma_0)$ and $v_n(\omega, \gamma_0)$ are the elastic and viscous Chebyshev coefficients, respectively, which are independent of each other. These coefficients are related: $e_n = G'_n(-1)^{(n-1)/2}$ and $v_n = \frac{G''_n}{\omega} = \eta'_n$, for n odd in both cases. The third harmonic Chebyshev coefficients are needed to interpret the nature of elastic and viscous nonlinearities. $e_3 > 0$ corresponds to strain-stiffening in the intracycles of the elastic stress, whereas $e_3 < 0$ specifies the strain-softening ones. Likewise, $v_3 > 0$ represents shear-thickening in the intracycles of the viscous stress, and $v_3 < 0$ describes the shear-thinning ones. This physical interpretation is not apparent in the time domain with the Fourier coefficients but becomes immediately apparent from the sign of the Chebyshev coefficients. Consequently, the first-harmonic coefficients in Eqs. (7) and (8) measure the average elasticity or dissipation per cycle in the material response at each imposed pair of LAOS coordinates (ω, γ_0), but they cannot represent the local elastic response of materials at small and large instantaneous strains nor differentiate between any local changes

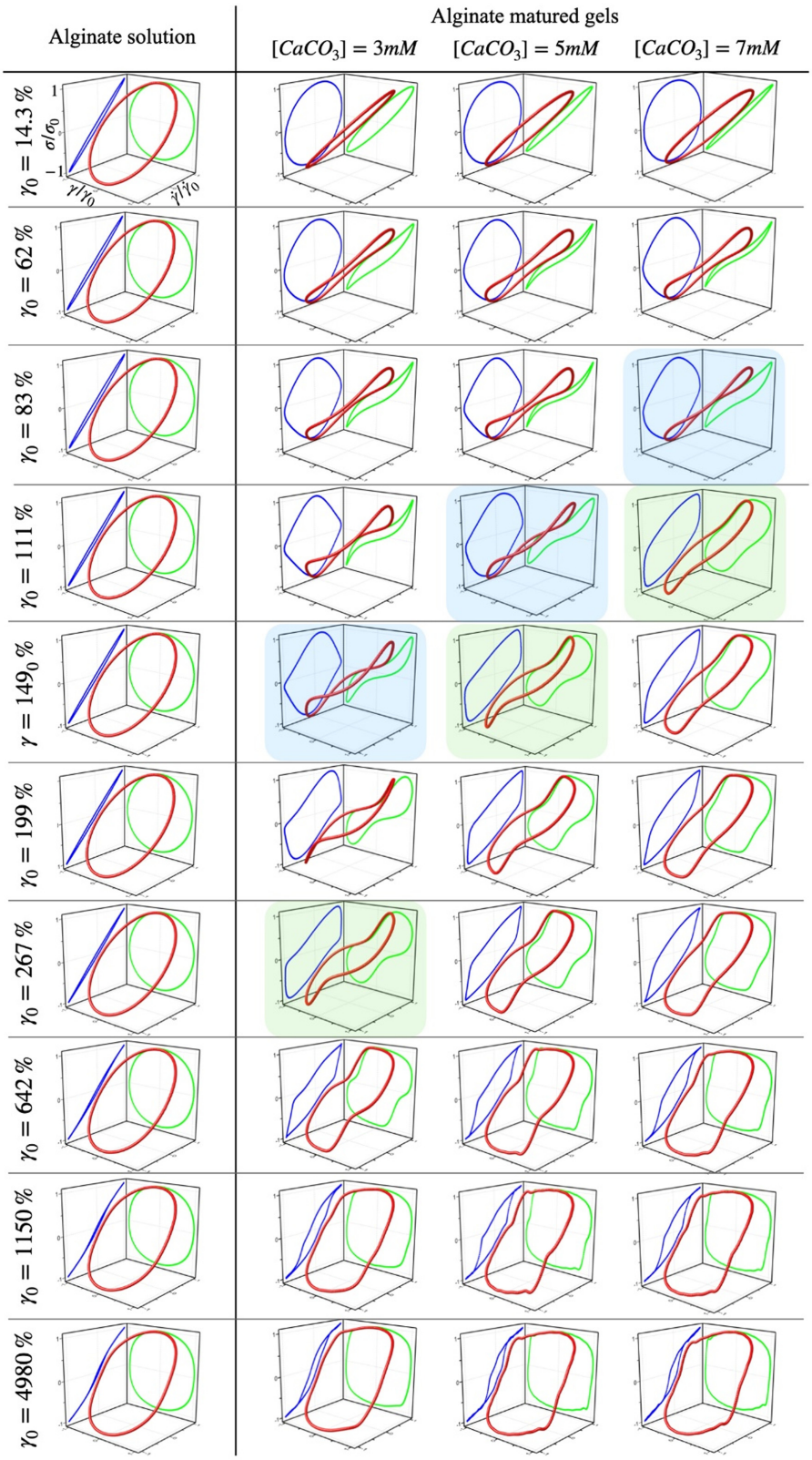

FIG. 4. Normalized 3D Lissajous–Bowditch curves and their projections (elastic representation: σ/σ_0 vs γ/γ_0 in green and viscous representation: σ/σ_0 vs. $\dot{\gamma}/\dot{\gamma}_0$ in blue) for an alginate solution and several matured alginate gels for different γ_0 ($C_{alginate} = 1.8$ w/v %, $C_{GDL} = 6$ mg/mL, and $[CaCO_3] = 3$, 5, and 7 mM at 25 °C). Blue shadow corresponds to $\gamma_0 = \gamma_{break}$, and green shadow corresponds to γ_0 where $G'(\gamma_o) \sim G''(\gamma_o)$.

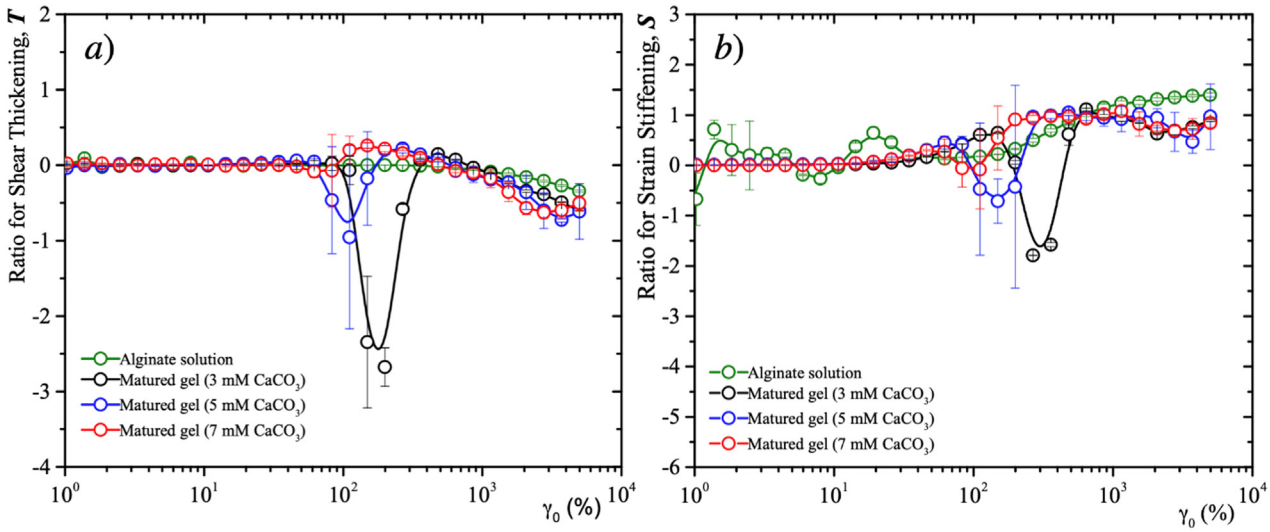

FIG. 5. Shear thickening (T) and ratio for strain stiffening (S) ratios vs γ for alginate solution ($C_{alginate} = 1.8$ w/v %) and alginate matured gels ($C_{alginate} = 1.8$ w/v %, $C_{GDL} = 6$ mg/mL, and $[CaCO_3] = 3$, 5, and 7 mM at 25 °C) at 25 °C. For each intracycle strain, the experiments were performed at $\omega = 1$ rad s^{-1}. Lines are a guide for the eye.

in the coefficient of viscous dissipation between the lowest and highest instantaneous shear rates experienced during an oscillatory deformation. To get a better physical insight, it is necessary to introduce new parameters to quantify intracycle nonlinearities that distort the linear viscoelastic ellipse, as the strain-stiffening ratio (S) and shear-thickening ratio (T) defined as[48]

$$S = \frac{G'_L - G'_M}{G'_L}, \tag{9}$$

$$T = \frac{\eta'_L - \eta'_M}{\eta'_L}. \tag{10}$$

For the strain-stiffening ratio, $G'_L \equiv \frac{\sigma}{\gamma}|_{\gamma=\pm\gamma_0} = \sum_{n\,odd} G'_n (-1)^{(n-1)/2} = e_1 + e_3 + \cdots$ is the large-strain modulus at the maximum imposed strain, and $G'_M \equiv \frac{d\sigma}{d\gamma}|_{\gamma=0} = \sum_{n\,odd} nG'_n = e_1 - 3e_3 + \cdots$ is the minimum-strain modulus at $\gamma = 0$. For the shear-thickening ratio, $\eta'_L \equiv \frac{\sigma}{\dot{\gamma}}|_{\dot{\gamma}=\pm\dot{\gamma}_0} = \frac{1}{\omega}\sum_{n\,odd} G''_n = v_1 + v_3 + \cdots$ is the large-shear rate dynamic viscosity, and $\eta'_M \equiv \frac{d\sigma}{d\dot{\gamma}}|_{\dot{\gamma}=0} = \frac{1}{\omega}\sum_{n\,odd} nG''_n (-1)^{\frac{n-1}{2}} = v_1 - 3v_3 + \cdots$ is the minimum-rate dynamic viscosity.[48] Different authors have discussed the geometrical decomposition of shear stress.[34,42,45,48,74]

The rheological response is linear when $S = 0$ and $T = 0$, as described in Ref. 48. $S > 0$ and $T > 0$ represent strain-stiffening and shear-thickening in the intracycles, respectively. For negative values, $S < 0$ represents strain-softening and $T < 0$ shear-thinning in the intracycles. Figure 5 shows the S and T parameters determined using the RheoCompass Software (Anton Paar, Austria). For the alginate solution, $S = 0$ and $T = 0$ in the LVR ($\gamma_0 \lesssim 46\%$), and as γ_0 increases, the shear-thickening ratio presents negative values, i.e., the material is shear thinning, in agreement with the discussion above (see Fig. 3). Regarding strain-stiffening ratio, S slightly oscillates around zero in the LVR. For higher strains, $S > 0$ increases with a positive curvature; this stiffening effect indicates a strong interaction among polymer chains that avoid alignment during shear deformation.[34,48] For all alginate/Ca^{+2} matured gels, $S = 0$ and $T = 0$ in the LVR at low strain ($\gamma_0 < 14\%$). In a second stage, increasing the strain beyond the LVR, both T and S decrease to negative values until a minimum; here, the intracycles are shear thinning and strain softening, consistent with a yielding process where the polymer chains are probably stretching. Subsequently increasing γ_0, although T and S are negative, they grow up until reaching a small maximum positive value; here, the shear thinning and strain softening are reduced as if the network junctions are trying to maintain the superstructure.[75] After that maximum, the network is broken; as the deformation increases, T becomes more negative, i.e., the shear-thinning is similar to alginate solutions. S is slightly positive; however, this small strain-stiffening is lost, increasing γ_0 beyond the positive maximum, similar to the strain softening in hydrogels.[44] The values of the mentioned minimum and maximum approximately correspond to the breakpoint and the cross point between $G'(\gamma)$ and $G''(\gamma)$ (see Fig. 2), respectively. These effects of shear-thinning and strain-thinning are larger for lower Ca^{2+} concentrations, which is associated directly with the density of cross-linking points in the network that increases with $[Ca^{2+}]$. At the highest γ_0 (~4980%), S and T ratios for broken gels are essentially the same. When comparing the alginate/Ca^{2+} gels *ex situ* created by Goudoulas *et al.*[42] ($C_{alginate} = 2$ wt. %, $[CaCl_2] = 100$–200 mM) with our *in situ* gels, we observed notable differences in the nonlinear viscoelastic behavior, specifically in terms of T and S ratios. In their study, the S and T curves did not exhibit convexity, contrary to our results, where the minima of T and S took negative values. Unlike the gels studied by Goudoulas *et al.*,[42] our results show a weak formation of temporary network junctions during the breaking process, which contrasts with the behavior of gels made of alginate, gelatin,[45] and alginate-gelatin in a layer.[42]

D. Kinect of gelation using DWS–microrheology

Figure 6(a) shows the MSDs for microspheres embedded in an alginate solution ($C_{alginate} = 1.8$ w/v %) at 25 °C determined from the electric field time correlation function coming the scattered light using DWS [see the inset of Fig. 6(a)]. Experimental MSD data were fit with a two-term power function ($\langle \Delta r^2(t) \rangle = A_1 \cdot t^{\alpha_1} + A_2 \cdot t^{\alpha_2}$), which is shown as a continuous red curve in Fig. 6(a). At short times ($t \lesssim 5 \times 10^{-3}$ s), the first slope is ~ 0.28, which corresponds to a subdiffusive motion ($ln\langle \Delta r^2(t) \rangle = ln\ 6D + \alpha_1\ ln\ t$); D is a diffusive coefficient). Here, the interaction of particles with the polymer chains limits their displacements mainly elastically, as described by the linear viscoelastic spectra at high frequencies. For long times ($t \gtrsim 5 \times 10^{-2}$ s), the tracer particle describes simple diffusion with a slope = 0.98; here, the alginate solution is mainly viscous. This behavior has been reported for synthetic polymers.[68,76] We can identify a relaxation time, τ, from the cross point between these two different diffusive regions: a subdiffusive one [$\langle \Delta r^2(t) \rangle \sim t^{0.28}$; green dashed line in Fig. 6(a)] and a simple diffusive [$\langle \Delta r^2(t) \rangle \sim t$); pink dashed line in Fig. 6(a)]. This method would be exact for a Maxwellian fluid with a single relaxation time.[76,77] However, in our case, the polymer chains present several relaxation modes operating when $t \gtrsim \tau$ as reptation, contour of length fluctuations, intra-tube Rouse modes, etc.[24,25] When a sol-gel transition starts, the value of τ changes due to the formation of the infinite gel network, as discussed below. Figure 6(b) shows the viscoelasticity spectra obtained from the MSDs of the mentioned alginate solution, as described in Sec. II D. Here, microrheology and mechanical rheology agree, validating our procedure. High-frequency rheology is similar to solutions of synthetic polymers,[68,76,77] and biopolymers.[51–54,59] From viscoelastic moduli crossover, a relaxation time τ_r ($=1/\omega_0 = 0.001$ s), an order of magnitude less than $\tau = 0.021$ s, can be obtained.

Figure 7 shows the MSD of PS tracer microspheres embedded in alginate solutions using the DWS technique measured at different times after starting gelation due to the Ca^{+2} release, following Sec. II D. Tracer motion shows the evolution from a sol to a gel as time elapses since gelation started. The MSD curves present a similar behavior for different Ca^{2+} concentrations. The elapsed time since gelation started will be named t_q. As gelation progresses, the diffusive region section, with a slope $\sim$1, decreases as t_q increases. As an example, for $[CaCO_3] = 3$ mM alginate solution [see Fig. 7(a)] at $t_q < 160$ min, tracers move similarly to the polymer solution described above, showing two slopes at short and long times. However, when $t_q \sim 160$ min, the diffusive region section has disappeared (the slope of the MSD curves is far from $m < 1$), i.e., the motion of the tracers is not diffusive anymore. Here, G' dominates, and particles are trapped since MSDs show the onset of a plateau that will be more pronounced as the number of network bonds increases, which is a function of Ca^{+2} concentration. The higher concentration of Ca^{2+} ions leads to multiple egg-box structures. The measured MSD curves were fitted as before with a two-term power function ($\langle \Delta r^2(t) \rangle = A_1 t^{\alpha_1} + A_2 t^{\alpha_2}$), imposing $a_2 = 1$. In this way, it is easy to observe clearly how the size of the diffusive region decreases as time elapses. For $t \gg \tau$, motion is diffusive. Therefore, the crossing point given by τ, which is a function of t_q, can help to estimate the gelation time for each alginate Ca^{2+} solution due to the change of curvature of the MSD curves. We expect that the gelation time corresponds approximately to where the diffusive region disappears, i.e., where a terminal relaxation time is reached. Here, the incipient gel network hinders particle motion and limits polymer reptation. As t_q increases and the gel matures, particle motion is confined, and there is no polymer reptation.[24,25] After 24 h of gelation, mean square displacement curves show the onset of a plateau, indicating an important particle confinement. Also, the slope at short times decreases according to increases in the Ca^{2+} ions, showing an increase in elasticity. This is consistent with the dependence of elasticity modulus with $[CaCO_3]$ (see Table II). Figure S5 in the supplementary material shows the viscoelastic spectra for all alginate/Ca^{2+} solutions, at high frequencies, for different t_q before they reach the gel state evaluated from their MSD

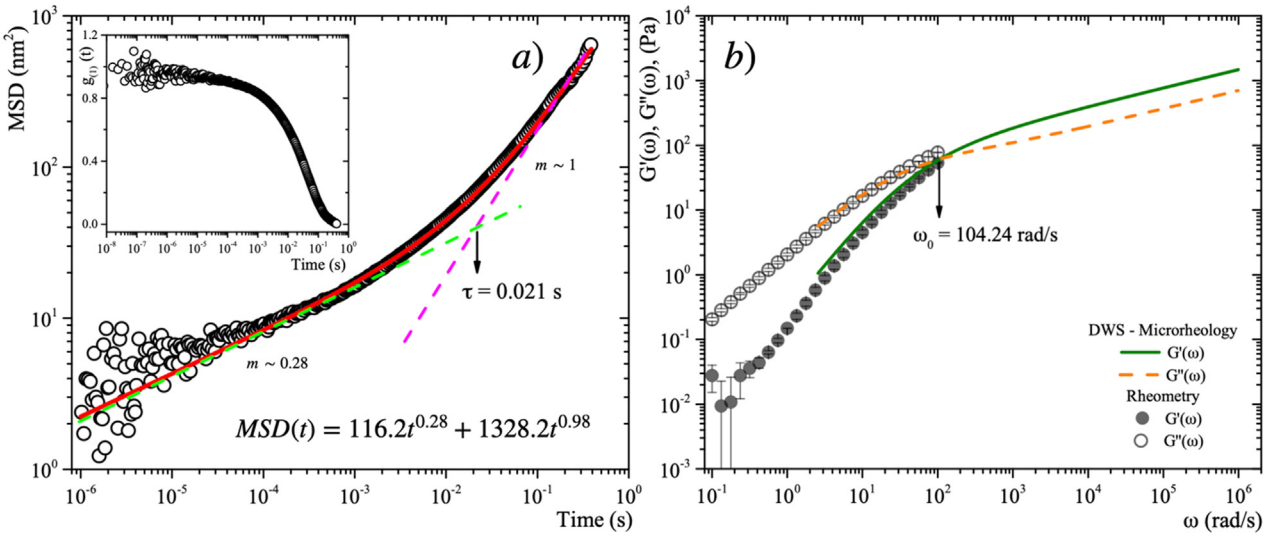

FIG. 6. Microrheology of an alginate solution with $C_{alginate} = 1.8$ w/v % at 25 °C. (a) MSD vs time for microspheres embedded in the alginate solution (dia. 784 nm and vol. fraction 0.025); open circles correspond to experimental MSD data, and continuous lines correspond to the best fit to a two-term power function: $\langle \Delta r^2(t) \rangle = A_1 \cdot t^{\alpha_1} + A_2 \cdot t^{\alpha_2}$ and $R^2 = 0.99$. Inset: Scattered light electric field correlation function vs t. (b) Viscoelastic spectra from MSD (DWS microrheology) and mechanical rheometry.

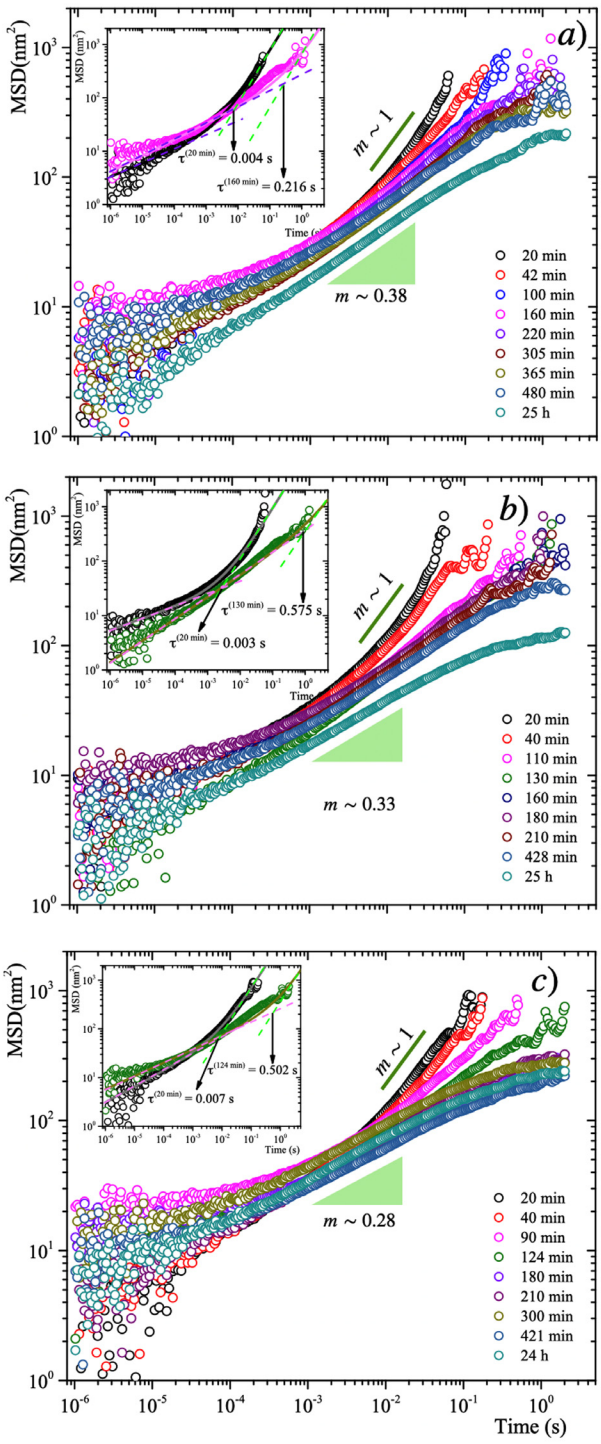

FIG. 7. MSD vs t for microspheres embedded in alginate solution ($C_{alginate} = 1.8$ w/v % and $C_{GDL} = 6$ mg/mL) for different times after starting the gelation varying the quantity of $CaCO_3$ at 25 °C: (a) $[CaCO_3] = 3$ mM, (b) $[CaCO_3] = 5$ mM, and $[CaCO_3] = 7$ mM. The insets show the last τ that can be determined because the diffusive region is nearly vanishing; the continuous line corresponds to bets fitting using a two-term power function, $\langle \Delta r^2(t) \rangle = A_1 t^{\alpha_1} + A_2 t$, with $R^2 \geq 0.98$ for all cases.

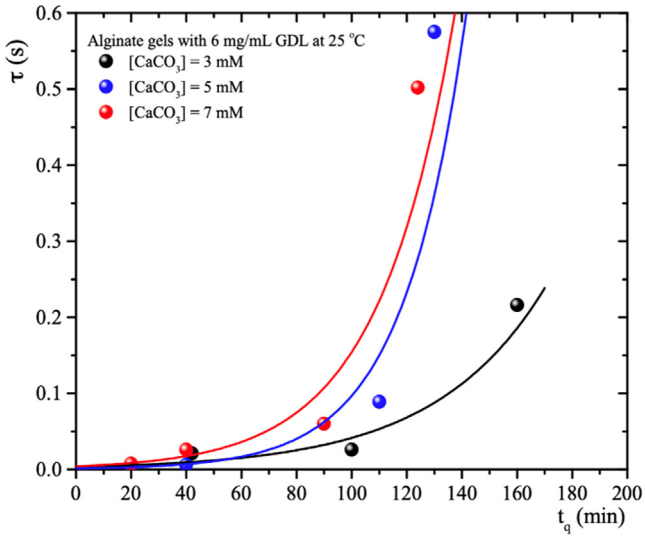

FIG. 8. τ vs t_q at different times after starting the gelation, varying the quantity of $CaCO_3$ at 25 °C. Continuous lines correspond to fitting to exponential curve; $\tau = 0.0034\ \exp(t_q/40)$ for $[CaCO_3] = 3$ mM (black curve, $R^2 = 0.98$); $\tau = 0.0012\ \exp(t_q/22.8)$ for $[CaCO_3] = 5$ mM (blue curve, $R^2 = 0.93$), and $\tau = 0.0041\ \exp(t_q/27.5)$ for $[CaCO_3] = 7$ mM (red curve, $R^2 = 0.97$).

curves. These viscoelastic spectra are similar to those of alginate solutions [see Fig. 6(b)]. However, as the gelation process evolves, i.e., as increases t_q, the cross point between $G'(\omega)$ and $G''(\omega)$ moves to low frequencies and the interval where $G'(\omega) > G''(\omega)$ increases. $G''(\omega) > G'(\omega)$ disappears due to the formation of the infinite network. This displacement follows a similar trend as the τ displacement, which moves at long times according to increasing t_q.

Figure 8 shows the evolution of the crossing point given by τ as a function of t_q for the different alginate/Ca^{+2} solutions, which follows approximately an exponential curve [$\tau = A\ \exp(t_q/T)$], A and T are fitting constants. Gelation times are ~160, ~130, and ~124 min for Ca^{2+} ions concentrations of 3, 5, and 7 mM, respectively. They correspond to the last τ points that can be measured due to the vanishing of the diffusion region (terminal relaxation time). The evolution of τ is similar for higher Ca^{2+} concentrations due to the formation of many multiple egg-box structures, in contrast to that for lower Ca^{2+} ions, where τ evolution is slow. The exponential decay of τ suggests a kinetic process of first order according to thermodynamics out of equilibrium where τ corresponds to the extent of the reaction,[78] in agreement with Funami *et al.*[79] These authors proposed a first-order kinetic equation to describe the temporal evolution of the storage modulus. Our mesoscopic results suggest that the evolution of the elasticity given during gelation follows the same kinetics process where reptation chain modes are disappearing, and G' is growing, adequately describing the network's evolution during the gelation process.

IV. CONCLUSIONS

We studied the linear and nonlinear rheological properties of alginate/Ca^{2+}gelation and how Ca^{2+} modifies them. At the critical point, as expected, $G'(\omega)$ and $G''(\omega)$ follow a power law with an exponent $n = 0.60$–0.65, which decreases slightly with increasing Ca^{2+}. The strain-hardening of the matured alginate gels at large

strains shows an overshot in $G'(\gamma_o)$ and $G''(\gamma_o)$ near the breaking point. Using the BST scaling model, $d_f \sim 1.23$–1.31, whose values are close to $d_f \sim 1.25$ for alginate beads using $[CaCl_2] = 100$ mM.[69] The fractal dimension is not affected by Ca^{2+}. The Lissajous–Bowditch curves show a higher nonlinearity and constitute a rheological fingerprint of these gels. These curves are similar at very high strains, indicating that the gel network is destroyed no matter the Ca^{2+} concentration. The geometrical decomposition of the intracycle strain in terms of strain-stiffening and shear-thickening ratios shows that prior to the breakpoint, we observe a sink whose bottom is at the breakpoint. Increasing the strain, although T and S are negative, they grow up until reaching a small positive maximum value corresponding to the $G'(\gamma_o)$ and $G''(\gamma_o)$ cross point, indicating temporary weak network junctions. After that maximum, the network is broken. As the deformation increases, T becomes more negative, the shear-thinning is similar to alginate solutions, and S is slightly positive but fades away.

The MSDs of tracer particles during the gelation of alginate/Ca^{2+} solutions exhibit a subdiffusive process, with two slopes in the MSD curves: a first slope of $\sim$0.3 at short times and a second slope of $\sim$1 at longer times. As gelation progresses, due to the slow release of Ca^{2+}, the diffusive region section decreases and finally disappears when the gels are formed; here, the gel network hinders particle motion and limits polymer reptation. We identified a relaxation time from the cross point between these different diffusive regions, which evolves as a fast-increasing exponential curve that is quite similar for the cases of high Ca^{2+} concentrations due to the formation of many multiple egg-box structures, in contrast to the case with low Ca^{2+} ions, where this relaxation time slowly grows. At long times, the MSD's curves develop a plateau, indicating important particle confinement and an increase in elasticity consistent with the increase in Ca^{2+}.

Our results contribute to the best knowledge about the linear and nonlinear rheological response for biopolymer gels whose gelation mechanism involves egg-box structures.[13] We expect that the nonlinear viscoelastic response and its link to the microstructure discussed here could help improve food quality and better understand processing issues.

SUPPLEMENTARY MATERIAL

See the supplementary material for the details of the molecular structure of the alginate chain, a cartoon of egg-box structure formation in the presence of Ca^{2+}, images of matured gels, isothermal time sweep curves, and linear viscoelastic spectra for alginate matured gels using rheometry and microrheology.

ACKNOWLEDGMENTS

Financial support from SEP CONAHCYT (A1-S-15587), DGAPAUNAM (IN 104024), and CONAHCYT scholarship for R. F. L-S are gratefully acknowledged. We thank C. Garza and Brisa Arenas for their technical support.

AUTHOR DECLARATIONS

Conflict of Interest

The authors have no conflicts to disclose.

Author Contributions

Ricky F. López-Santiago: Conceptualization (equal); Formal analysis (equal); Investigation (equal); Writing – original draft (equal); Writing – review & editing (equal). **Rolando Castillo:** Conceptualization (equal); Formal analysis (equal); Funding acquisition (equal); Investigation (equal); Writing – original draft (equal); Writing – review & editing (equal).

DATA AVAILABILITY

The data supporting this study's findings are available from the corresponding author upon reasonable request.

REFERENCES

[1] A. Linker and R. S. Jones, "A polysaccharide resembling alginic acid from a pseudomonas micro-organism," Nature **204**, 187–188 (1964).
[2] A. Linker and R. S. Jones, "A new polysaccharide resembling alginic acid isolated from pseudomonads," J. Biol. Chem. **241**(16), 3845–3851 (1966).
[3] M. S. Hasnain, E. Jameel, B. Mohanta, A. K. Dhara, S. Alkahtani, and A. K. Nayak, "Alginates: Sources, structure, and properties," in *Alginates in Drug Delivery* (Elsevier, 2020), pp. 1–17.
[4] Y. Qin, J. Jiang, L. Zhao, J. Zhang, and F. Wang, "Applications of alginate as a functional food ingredient," in *Biopolymers for Food Design* (Elsevier, 2018), pp. 409–429.
[5] Y. Qin, J. Jiang, L. Zhao, J. Zhang, and F. Wang, *Polymer Based Systems on Tissue Engineering, Replacement and Regeneration* (Springer Netherlands, Dordrecht, 2002).
[6] I. A. Brownlee, A. Allen, J. P. Pearson, P. W. Dettmar, M. E. Havler, M. R. Atherton, and E. Onsøyen, "Alginate as a source of dietary fiber," Crit. Rev. Food Sci. Nutr. **45**(6), 497–510 (2005).
[7] K. Adamiak and A. Sionkowska, "State of innovation in alginate-based materials," Mar. Drugs **21**(6), 353 (2023).
[8] I. A. Brownlee, C. J. Seal, M. Wilcox, P. W. Dettmar, and J. P. Pearson, "Applications of alginates in food," in *Alginates: Biology and Applications* (Springer, 2009), pp. 211–228.
[9] D. Li, Z. Wei, and C. Xue, "Alginate-based delivery systems for food bioactive ingredients: An overview of recent advances and future trends," Compr. Rev. Food Sci. Food Saf. **20**(6), 5345–5369 (2021).
[10] S. H. Ching, N. Bansal, and B. Bhandari, "Alginate gel particles–A review of production techniques and physical properties," Crit. Rev. Food Sci. Nutr. **57**(6), 1133–1152 (2017).
[11] F. Yokoyama, C. E. Achife, K. Takahira, Y. Yamashita, K. Monobe, F. Kusano, and K. Nishi, "Morphologies of oriented alginate gels crosslinked with various divalent metal ions," J. Macromol. Sci., Part B **31**(4), 463–483 (1992).
[12] D. Larobina and L. Cipelletti, "Hierarchical cross-linking in physical alginate gels: A rheological and dynamic light scattering investigation," Soft Matter **9**(42), 10005 (2013).
[13] L. Cao, W. Lu, A. Mata, K. Nishinari, and Y. Fang, "Egg-box model-based gelation of alginate and pectin: A review," Carbohydr. Polym. **242**, 116389 (2020).
[14] D. Bi, X. Yang, L. Yao, Z. Hu, H. Li, X. Xu, and J. Lu, "Potential food and nutraceutical applications of alginate: A review," Mar. Drugs **20**(9), 564 (2022).
[15] I. Ben Djemaa, F. Boulmedais, S. Auguste, M. Tarnowska, S. Andrieux, and W. Drenckhan-Andreatta, "Glucono-delta-lactone-induced alginate gelation: New insights into the effect of the cross-linker carrier type on the hydrogel mechanics," Langmuir **40**(20), 10492–10501 (2024).
[16] E. A. Growney Kalaf, R. Flores, J. G. Bledsoe, and S. A. Sell, "Characterization of slow-gelling alginate hydrogels for intervertebral disc tissue-engineering applications," Mater. Sci. Eng., C **63**, 198–210 (2016).
[17] K. I. Draget, "Alginates," in *Handbook of Hydrocolloids* (Elsevier, 2009), pp. 807–828.
[18] C. Bennacef, S. Desobry-Banon, L. Probst, and S. Desobry, "Advances on alginate use for spherification to encapsulate biomolecules," Food Hydrocolloids **118**, 106782 (2021).

[19]B. F. Gibbs, S. Kermasha, I. Alli, and C. N. Mulligan, "Encapsulation in the food industry: A review," Int. J. Food Sci. Nutr. **50**(3), 213–224 (1999).
[20]Y. Weng, G. Yang, Y. Li, L. Xu, X. Chen, H. Song, and C.-X. Zhao, "Alginate-based materials for enzyme encapsulation," Adv. Colloid Interface Sci. **318**, 102957 (2023).
[21]K. Suman and Y. M. Joshi, "On the universality of the scaling relations during sol-gel transition," J. Rheol. **64**(4), 863–877 (2020).
[22]F. Chambon and H. H. Winter, "Linear viscoelasticity at the gel point of a crosslinking PDMS with imbalanced stoichiometry," J. Rheol. **31**(8), 683–697 (1987).
[23]H. H. Winter, "Gel point," in *Encyclopedia of Polymer Science and Technology* (Wiley, 2016), pp. 1–15.
[24]M. Rubinstein and R. H. Colby, *Polymer Physics* (Oxford University Press, Oxford, 2003).
[25]P.-G. de Gennes, *Scaling Concepts in Polymer Physics* (Cornell University Press, Ithaca and London, 1997).
[26]Lu, X. Liu, L. Dai, and Z. Tong, "Difference in concentration dependence of relaxation critical exponent n for alginate solutions at sol−gel transition induced by calcium cations," Biomacromolecules **6**(4), 2150–2156 (2005).
[27]X. Liu, L. Qian, T. Shu, and Z. Tong, "Rheology characterization of sol–gel transition in aqueous alginate solutions induced by calcium cations through in situ release," Polymer **44**(2), 407–412 (2003).
[28]S. Liu, H. Li, B. Tang, S. Bi, and L. Li, "Scaling law and microstructure of alginate hydrogel," Carbohydr. Polym. **135**, 101–109 (2016).
[29]H. Zheng, Q. Zhang, K. Jiang, H. Zhang, and J. Wang, "Critical behavior of viscosity for alginate solutions near the gelation threshold induced by cupric ions," J. Chem. Phys. **105**(17), 7746–7752 (1996).
[30]L. Lu, X. Liu, and Z. Tong, "Critical exponents for sol–gel transition in aqueous alginate solutions induced by cupric cations," Carbohydr. Polym. **65**(4), 544–551 (2006).
[31]R. Hernández, J. Sacristán, and C. Mijangos, "Sol/gel transition of aqueous alginate solutions induced by Fe^{2+} cations," Macromol. Chem. Phys. **211**(11), 1254–1260 (2010).
[32]G. Yazar, O. C. Duvarci, M. Y. Erturk, and J. L. Kokini, "LAOS (large amplitude oscillatory shear) applications for semisolid foods," in *Rheology of Semisolid Foods* (Springer, 2019), pp. 97–131.
[33]Y. Wang and C. Selomulya, "Food rheology applications of large amplitude oscillation shear (LAOS)," Trends Food Sci. Technol. **127**, 221–244 (2022).
[34]K. Hyun, M. Wilhelm, C. O. Klein, K. S. Cho, J. G. Nam, K. H. Ahn, S. J. Lee, R. H. Ewoldt, and G. H. McKinley, "A review of nonlinear oscillatory shear tests: Analysis and application of large amplitude oscillatory shear (LAOS)," Prog. Polym. Sci. **36**(12), 1697–1753 (2011).
[35]H. S. Melito, C. R. Daubert, and E. A. Foegeding, "Relationships between nonlinear viscoelastic behavior and rheological, sensory and oral processing behavior of commercial cheese," J. Texture Stud. **44**(4), 253–288 (2013).
[36]M. Y. Erturk, J. C. Bonilla, and J. Kokini, "Relationship of non-linear rheological properties and quantitative network analysis parameters as a function of increasingly large amplitude deformations in non-fat, low-fat and high-fat yogurt products," Food Hydrocolloids **111**, 106194 (2021).
[37]J. J. Griebler and S. A. Rogers, "The nonlinear rheology of complex yield stress foods," Phys. Fluids **34**(2), 023107 (2022).
[38]A. J. Sandoval, M. Fernández, O. Sanz, A. Santamaría, E. Penott-Chang, and A. J. Müller, "Large amplitude oscillatory shear (LAOS) behavior of chocolates of different compositions," J. Rheol. **66**(5), 859–879 (2022).
[39]P. Ptaszek, "Large amplitudes oscillatory shear (LAOS) behavior of egg white foams with apple pectins and xanthan gum," Food Res. Int. **62**, 299–307 (2014).
[40]R. J. Andrade, A. G. Azevedo, R. M. Musampa, and J. M. Maia, "Thermo-rheological behavior of model protein–polysaccharide mixtures," Rheol. Acta **49**(4), 401–410 (2010).
[41]M. Tang, Y. Lei, Y. Wang, D. Li, and L. Wang, "Rheological and structural properties of sodium caseinate as influenced by locust bean gum and κ-carrageenan," Food Hydrocolloids **112**, 106251 (2021).
[42]T. B. Goudoulas, A. Didonaki, S. Pan, E. Fattahi, and T. Becker, "Comparative large amplitude oscillatory shear (LAOS) study of ionically and physically crosslinked hydrogels," Polymers **15**(6), 1558 (2023).
[43]T. B. Goudoulas and N. Germann, "Phase transition kinetics and rheology of gelatin-alginate mixtures," Food Hydrocolloids **66**, 49–60 (2017).
[44]J. John, D. Ray, V. K. Aswal, A. P. Deshpande, and S. Varughese, "Dissipation and strain-stiffening behavior of pectin–Ca gels under LAOS," Soft Matter **15**(34), 6852–6866 (2019).
[45]T. B. Goudoulas and N. Germann, "Nonlinear rheological behavior of gelatin gels: In situ gels and individual layers," J. Colloid Interface Sci. **553**, 746–757 (2019).
[46]C. O. Klein, H. W. Spiess, A. Calin, C. Balan, and M. Wilhelm, "Separation of the nonlinear oscillatory response into a superposition of linear, strain hardening, strain softening, and wall slip response," Macromolecules **40**(12), 4250–4259 (2007).
[47]M. Wilhelm, "Fourier-transform rheology," Macromol. Mater. Eng. **287**(2), 83–105 (2002).
[48]R. H. Ewoldt, A. E. Hosoi, and G. H. McKinley, "New measures for characterizing nonlinear viscoelasticity in large amplitude oscillatory shear," J. Rheol. **52**(6), 1427–1458 (2008).
[49]P. J. Blatz, S. C. Sharda, and N. W. Tschoegl, "Strain energy function for rubberlike materials based on a generalized measure of strain," Trans. Soc. Rheol. **18**(1), 145–161 (1974).
[50]R. D. Groot, A. Bot, and W. G. M. Agterof, "Molecular theory of strain hardening of a polymer gel: Application to gelatin," J. Chem. Phys. **104**(22), 9202–9219 (1996).
[51]M. A. K. Williams, R. R. Vincent, D. N. Pinder, and Y. Hemar, "Microrheological studies offer insights into polysaccharide gels," J. Non-Newtonian Fluid Mech. **149**(1–3), 63–70 (2008).
[52]R. R. Vincent and M. A. K. Williams, "Microrheological investigations give insights into the microstructure and functionality of pectin gels," Carbohydr. Res. **344**(14), 1863–1871 (2009).
[53]B. Maciel, C. Oelschlaeger, and N. Willenbacher, "Chain flexibility and dynamics of alginate solutions in different solvents," Colloid Polym. Sci. **298**(7), 791–801 (2020).
[54]A. Varela-Feijoo, P. Djemia, T. Narita, F. Pignon, A. Baeza-Squiban, V. Sirri, and A. Ponton, "Multiscale investigation of viscoelastic properties of aqueous solutions of sodium alginate and evaluation of their biocompatibility," Soft Matter **19**(31), 5942–5955 (2023).
[55]R. F. López-Santiago, J. Delgado, and R. Castillo, "Competition among physical, chemical, and hybrid gelation mechanisms in biopolymers," Soft Matter **20**(11), 2518–2531 (2024).
[56]W. Hong, G. Xu, X. Ou, W. Sun, T. Wang, and Z. Tong, "Colloidal probe dynamics in gelatin solution during the sol–gel transition," Soft Matter **14**(19), 3694–3703 (2018).
[57]L. G. Rizzi, "Microrheological approach for the viscoelastic response of gels," J. Rheol. **64**(4), 969–979 (2020).
[58]T. H. Larsen and E. M. Furst, "Microrheology of the liquid-solid transition during gelation," Phys. Rev. Lett. **100**(14), 146001 (2008).
[59]Y. Hemar and D. N. Pinder, "DWS microrheology of a linear polysaccharide," Biomacromolecules **7**(3), 674–676 (2006).
[60]A. Tavera-Vázquez, N. Rincón-Londoño, R. F. López-Santiago, and R. Castillo, "Measuring mesoscopic scales in complex fluids embedded with giant cylindrical micelles with diffusing wave spectroscopy micro-rheology," J. Phys. Condens. Matter **34**(3), 034003 (2022).
[61]D. A. Weitz and D. J. Pine, "Diffusing-wave spectroscopy," in *Dynamic Light Scattering* (Oxford University Press, Oxford, 1993), pp. 652–720.
[62]A. Martinsen, G. Skjåk-Braek, O. Smidsrød, F. Zanetti, and S. Paoletti, "Comparison of different methods for determination of molecular weight and molecular weight distribution of alginates," Carbohydr. Polym. **15**(2), 171–193 (1991).
[63]U. Ritgen, *Analytical Chemistry I* (Springer, Berlin, Heidelberg, 2023).
[64]J. Galvan-Miyoshi, J. Delgado, and R. Castillo, "Diffusing wave spectroscopy in Maxwellian fluids," Eur. Phys. J. E **26**(4), 369–377 (2008).
[65]E. Sarmiento-Gomez, D. Lopez-Diaz, and R. Castillo, "Microrheology and characteristic lengths in wormlike micelles made of a zwitterionic surfactant and SDS in brine," J. Phys. Chem. B **114**(38), 12193–12202 (2010).
[66]N. Rincón-Londoño, C. Garza, N. Esturau-Escofet, A. Kozina, and R. Castillo, "Selective incorporation of one of the isomers of a photoswitchable molecule in wormlike micelles," Colloids Surf. A **610**, 125903 (2021).

[67]R. F. López-Santiago, J. Delgado, and R. Castillo, "Micellar entanglement and its relation to the elastic behavior of wormlike micelle fluids," J. Colloid Interface Sci. **626**, 1015–1027 (2022).
[68]E. Sarmiento-Gomez, I. Santamaría-Holek, and R. Castillo, "Mean-square displacement of particles in slightly interconnected polymer networks," J. Phys. Chem. B **118**(4), 1146–1158 (2014).
[69]J. E. Martin, D. Adolf, and J. P. Wilcoxon, "Viscoelasticity near the sol-gel transition," Phys. Rev. A **39**(3), 1325–1332 (1989).
[70]A. Posbeyikian, E. Tubert, A. Bacigalupe, M. M. Escobar, P. R. Santagapita, G. Amodeo, and M. Perullini, "Evaluation of calcium alginate bead formation kinetics: An integrated analysis through light microscopy, rheology and microstructural SAXS," Carbohydr. Polym. **269**, 118293 (2021).
[71]G. Harrison, G. V. Franks, V. Tirtaatmadja, and D. V. Boger, "Suspensions and polymers - Common links in rheology," Korea-Australia Rheol. J. **11**(3), 197–218 (1999).
[72]G. J. Donley, J. R. de Bruyn, G. H. McKinley, and S. A. Rogers, "Time-resolved dynamics of the yielding transition in soft materials," J. Non-Newtonian Fluid Mech. **264**, 117–134 (2019).
[73]G. J. Donley, M. Bantawa, and E. Del Gado, "Time-resolved microstructural changes in large amplitude oscillatory shear of model single and double component soft gels," J. Rheol. **66**(6), 1287–1304 (2022).
[74]M. Kamkar, R. Salehiyan, T. B. Goudoulas, M. Abbasi, C. Saengow, E. Erfanian, S. Sadeghi, G. Natale, S. A. Rogers, A. J. Giacomin, and U. Sundararaj, "Large amplitude oscillatory shear flow: Microstructural assessment of polymeric systems," Prog. Polym. Sci. **132**, 101580 (2022).
[75]D. Szopinski and G. A. Luinstra, "Viscoelastic properties of aqueous guar gum derivative solutions under large amplitude oscillatory shear (LAOS)," Carbohydr. Polym. **153**, 312–319 (2016).
[76]J. H. van Zanten, S. Amin, and A. A. Abdala, "Brownian motion of colloidal spheres in aqueous PEO solutions," Macromolecules **37**(10), 3874–3880 (2004).
[77]J. H. van Zanten and K. P. Rufener, "Brownian motion in a single relaxation time Maxwell fluid," Phys. Rev. E **62**(4), 5389–5396 (2000).
[78]D. Kondepudi and I. Prigogine, *Modern Thermodynamics* (Wiley, 2014).
[79]T. Funami, Y. Fang, S. Noda, S. Ishihara, M. Nakauma, K. I. Draget, K. Nishinari, and G. O. Phillips, "Rheological properties of sodium alginate in an aqueous system during gelation in relation to supermolecular structures and Ca^{2+} binding," Food Hydrocolloids **23**(7), 1746–1755 (2009).